Phase Separation and Crystallization Behavior of Poly(vinylidene fluoride)/ Poly(1,4-butylene adipate) Blends under an Electric Field

Jong Soon Lee,† Arun Anand Prabu, Kap Jin Kim,* and Cheolmin Park

Department of Advanced Polymer & Fiber Materials, College of Environment & Applied Chemistry, Kyung Hee University, Yongin-si, Gyeonggi-do 446-701, South Korea, and Department of Materials Science and Engineering, Yonsei University, Seoul 120-749, Korea

Received November 29, 2007; Revised Manuscript Received March 13, 2008

ABSTRACT: The effect of electric field on phase separation behavior and crystallization kinetics in binary semicrystalline blends of poly(vinylidene fluoride) (PVDF) and poly(1,4-butylene adipate) (PBA) has been investigated by means of time-resolved small-angle light scattering (SALS) and polarizing optical microscopy. PVDF/PBA blends are miscible in a temperature range between the melting point of PVDF and the LCST in the absence of an electric field. On the other hand, the binodal curve fitted with the cloud points obtained experimentally from SALS measurement was shifted toward lower temperature in the presence of the electric field. Thus, the field-induced phase separation and the field removal-induced phase dissolution could be observed reversibly for the 9/1 and 7/3 blends. Effects of various pretreatment conditions (spinodal phase separation time, field-induced phase separation, field removal-induced phase dissolution, etc.) of the PVDF/PBA blends before isothermal crystallization on the crystallization kinetics were also investigated.

I. Introduction

Binary polymer blends exhibit a wide variety of phase morphologies, and remarkable progress in polymer−polymer phase separation has been shown in the areas of thermodynamic phase equilibrium and kinetics of phase decomposition.[1,2] Though there are numerous reports on the kinetic aspects of phase separation and dissolution in amorphous−amorphous polymer blends,[3–6] very few studies have been reported on crystalline−amorphous polymer blends, and that too mostly on PVDF/PMMA blends.[7–9] In the case of crystalline−crystalline polymer blends, owing to the involvement of complex crystalline morphology and the crystallization behavior of the constituent polymers,[10–15] it is very difficult to interpret the physicochemical properties such as the phase diagram of polymer solution or polymer/polymer blend under an electric field using Gibbs free energy of mixing (ΔG_m), enthalpy of mixing (ΔH_m), or entropy of mixing (ΔS_m). Until now, there are very few studies on phase diagram and phase separation behavior under the electric field for polymer solutions and polymer−polymer blends.[16–20]

Among the many binary crystalline polymer blends, very few researchers have focused on poly(vinylidene fluoride) (PVDF)/ poly(1,4-butylene adipate) (PBA) blends and have reported the complete miscibility of PVDF with PBA over the entire composition range.[10,11,13,15] This miscibility behavior finds its origin from dipole−dipole interaction and/or hydrogen-bonding interactions. While PVDF/PMMA and PVDF/PVAc blends exhibit a typical lower critical solution temperature (LCST, >350 °C) much above the melting temperature of PVDF (ca. 178 °C),[8,21] the PVDF/PBA blend shows relatively lower LCST (ca. 235 °C).[10,11,15] When the cloud points of certain polymer blends are measured as a function of composition in the absence of an external electric field, the resulting data can be analyzed with the nonlinear least-squares curve-fitting method using a free energy of mixing (ΔG_m) which is expressed with only two terms, i.e., entropy of mixing and enthalpy of mixing. However, when the cloud points are measured under the electric field E, the data points cannot be fitted with a simple Flory−Huggins equation representing the free energy of mixing without an electric field, and hence the electrostatic free energy factor must be included in the equation. Therefore, the cloud point will be changed depending on the electric field strength at the same polymer blend compositions.When the electric field is applied to polymer solution, the Flory−Huggins parameter χ_c increases at critical concentration ϕ_c with increasing electric field strength, resulting in lower upper critical solution temperature (UCST) and higher LCST.[16,17] As an evidence toward this thought, Wirtz et al. suggested and validated their theory by simultaneously studying the phase behavior of polystyrene/cyclohexane mixture and poly(*p*-chlorostyrene)/ethylcarbitol mixture solutions under the electric field through laser light scattering.[16,17] Using theoretical equations quite different from Wirtz and Fuller's equation, Gurovich[18–20] predicted that the critical temperature in polymer solution or polymer−polymer blend is lowered with increasing electric field for UCST. Overall, the above reports were used to confirm the contribution of electric field toward increasing miscibility of polymer solution or blends at the interface region regardless of UCST and LCST behavior.[16–20]

In the present study, the effect of electric field on phase separation behavior and crystallization kinetics in PVDF/PBA blends has been investigated. LCST behavior under the electric field was examined on the basis of a new theoretical equation along with experimental studies, and the results are discussed in detail.

II. Experimental Section

Materials and Sample Preparation. PVDF resin (Kynar 761, M_w = 480 000, Atofina Co.) as electroactive polymer and poly(1,4-butylene adipate) (PBA, M_w = 12 000, Scientific Polymer Products) as electroinactive polymer were used as received. PVDF and PBA were dissolved separately in *N,N*-dimethylformamide (DMF) used as cosolvent. Each of 4 wt % stock solutions was subsequently mixed with varying PVDF/PBA composition ratios and then precipitated in copious amounts of deionized water. The precipitate was washed many times with deionized water to remove the residual solvent, and the products were dried in vacuum oven for 5 days at 85 °C. About 50 μm thick films of each PVDF blend were obtained through melt-pressing the powdered samples using a Carver press, and the films were quenched in iced water. The dried blend films

* Corresponding author: Ph +82-31-201-2518; Fax +82-31-204-8114; e-mail kjkim@khu.ac.kr.

† Present address: Analytical Research Center, Hyosung R&DB Labs, Anyang-si, Gyeonggi-do 431-080, South Korea.

10.1021/ma702655n CCC: $40.75
Published on Web 05/03/2008

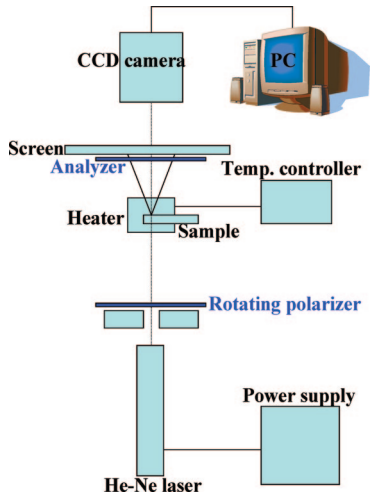

Figure 1. Schematic diagram of a time-resolved 2-D laser light scattering apparatus.

were placed between two glass slides having a transparent ITO conducting layer in their inner surfaces and used for further measurements.

Cloud Point Measurement. The cloud point measuring apparatus used in this study is fitted with a 5 mW He−Ne laser light (λ = 632.8 nm) source (05 LHR 151, Melles-Griot, Netherlands), a custom-made heating stage controlled by a programmable temperature controller (CN2001, Omega Technologies Co.), and a goniometer equipped with photodiode (Model DET110/M, Thorlabs Inc.). The scattered light was detected at the photodiode placed 10° apart from incident light. The cloud point was measured during heating (1 °C/min) under the desired electric field (0−9 MV/m), and an abrupt change in scattered intensity caused by phase separation during heating was regarded as a cloud point.

Time-Resolved 2-D Small-Angle Light Scattering (SALS) Measurement. A Kapton spacer film was placed around the prepared sample to prevent electrical shortage caused by air under an external electric field (0−7 MV/m). As shown in Figure 1, the SALS apparatus consists of a 5 mW He−Ne laser light (λ = 632.8 nm) source (05 LHR 151, Melles-Griot, The Netherlands), a custom-made hot stage controlled by a programmable temperature controller (CN2001, Omega Technologies Co.), a semitransparent white screen with an analyzer beneath it, a rotary polarizer controlled by a stepping motor, and a 2-D CCD camera (Orbis16, pixels 1280 × 1024, 16-bit resolution, Spectra Source Instruments) to capture the scattered image on the screen. For temperature-jump (T-jump) experiments, an additional hot stage was used for preheating the specimen at a single-phase temperature of 220 °C for 15 min. As soon as the specimen was rapidly transferred from the preheating hot stage to the hot stage on the light scattering apparatus kept at the desired temperature above the melting temperature, the scattering pattern by a spinodal phase separation was recorded and saved in a personal computer as a function of time. Two optical geometries were adopted. One is the H_V geometry for the observation of crystallization behavior, and the other is the V_V geometry for the observation of both crystallization and liquid−liquid phase separation. When the V_V scattering profiles were measured, a neutral density filter, whose optical density is 2, was inserted into the laser light beam path to attenuate the intensity of the incident laser light and for the purpose of reducing parasitic scattering.

Polarizing Optical Microscopy (POM) Observation. Isothermal melt-crystallization behavior in the presence of an electric field was carried out using a POM (Nikon Optiphot-POL) equipped with a Mettler FP82 hot stage, a photodetector, and a Watec CCD camera. The distance between the ITO electrodes was adjusted to be around 30 μm by placing Kapton film spacers around the sample. After melting at 210 °C for 15 min under an external electric field (0−5 MV/m), each sample was quenched to the desired isothermal temperature between 150 and 162 °C at the maximum cooling rate allowed. The microscopic image displayed on the monitor was saved in order to observe and analyze the crystalline morphology, and the transmitted light intensity under cross-polarization was also recorded simultaneously as a function of crystallization time in order to evaluate the crystallization rate. The high-voltage supplier used was a PMT-75C model manufactured by Bertan Co. To get the phase separation microscopic image under the electric field, the optical microscopic images were observed with a parallel polarization, and the iris diaphragm of the Abbe condenser nearly closed. The temperature adopted for the T-jump experiment in this study was similar to that used previously in the SALS measurement.

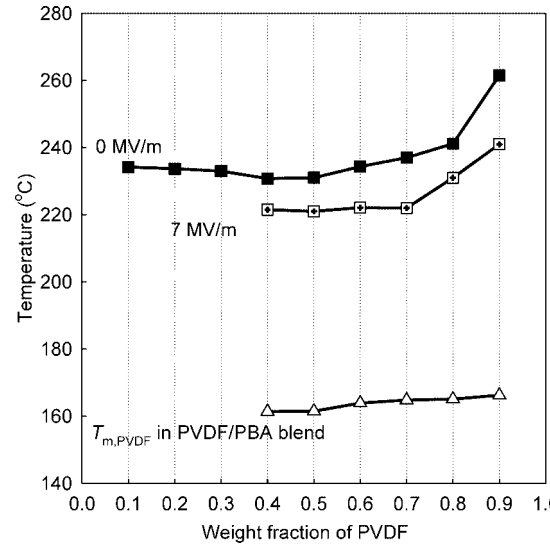

Figure 2. Phase diagram of PVDF/PBA blend.

DSC Measurement. To analyze the melting behavior of samples that have been previously subjected to melting and different isothermal crystallization conditions, DSC curves were obtained under a nitrogen atmosphere with a heating rate of 10 °C/min using a Perkin-Elmer DSC-4 differential scanning calorimeter (DSC) calibrated with the melting temperature of indium.

III. Results and Discussion

Phase Diagram and Binodal Curve under an External Electric Field. The phase diagram of PVDF/PBA blends obtained from cloud point measurement is depicted in Figure 2. PVDF/PBA blends are apparently miscible in a temperature range between the melting point of PVDF and the LCST. In general, the melting point depression occurs for miscible crystalline/amorphous polymer blend or miscible blend of crystalline (A) polymer and crystalline (B) polymer blend exhibiting lower melting point than that of polymer (A). From melting point depression, the interaction energy density B between polymers and Flory−Huggins interaction parameter χ can be determined.[7] With increasing melting point depression, B and χ have considerably large negative values. On the basis of the dipole−dipole interaction, most of miscible blends show the LCST behavior. At higher LCST, the interaction energy between two polymers becomes higher. As shown in Figure 2, PVDF/PBA blends exhibit traditional LCST behavior in the absence of an applied electric field. On the other hand, the cloud points of the PVDF/PBA blends were depressed with electric field, and these phenomena are quite opposite to that predicted by Wirtz−Fuller[17] and Gurovich;[20] i.e., LCST rises with increasing the electric field. On the basis of the Wirtz−Fuller equation,[17] the reason for LCST depression with increasing electric field cannot be explained but can be explained to some extent based on Gurovich's equation.[20]

Following Gurovich's equation representing the free energy of mixing per segment for binary polymer blend composed of polymer chains 1 and 2, whose degrees of polymerization are x_1 and x_2, respectively, under an electric field (E), one can write the equation[20]

$$\frac{\Delta G_m(\phi,E)}{kT} = \left[\frac{\phi}{x_1}\ln\phi + \frac{1-\phi}{x_2}\ln(1-\phi)\right] + \chi\left(1-\frac{E^2}{\langle F^2\rangle}\right)\phi(1-\phi) \quad (1)$$

where ϕ and $1-\phi$ are volume fraction of the monomers 1 and 2, respectively, ϕ is the Flory−Huggins interaction parameter, k is the Boltzmann constant, T is the temperature, and $\langle F^2\rangle$ is the mean-squared spontaneously fluctuating molecular electric field. Since the electric field strength (E) applied in this work is 5−9 MV/m and the spontaneously fluctuating molecular electric field (F) has the range between 100 and 10 000 MV/m, the Flory−Huggins parameter is insensitive to an applied field.[20]From the condition satisfying $\partial^2\Delta G_m(\phi,E)/\partial\phi^2 = 0$ and $\partial^3\Delta G_m(\phi,E)/\partial\phi^3 = 0$ simultaneously, the critical volume fraction $\phi_c(E)$ and the critical Flory−Huggins parameter $\chi_c(E)$ under the field can be obtained from eqs 2 and 3, respectively.

$$\phi_c(E) = \frac{x_2^{1/2}}{x_1^{1/2}+x_2^{1/2}} = \phi_c \quad (2)$$

$$\chi_c(E) = \frac{(x_1^{1/2}+x_2^{1/2})^2}{2x_1x_2\left(1-\frac{E^2}{\langle F^2\rangle}\right)} = \frac{\chi_c}{1-\frac{E^2}{\langle F^2\rangle}} \quad (3)$$

Under the assumption that the interaction parameter is a simple function of inverse absolute temperature, i.e., $\chi(T) = a + b/T$ ($a < 0$ and $b > 0$ for UCST; $a > 0$ and $b < 0$ for LCST),[1,11] the critical temperature under the field, $T_c(E)$, can be obtained from eq 4 derived with a combination of eq 3.

$$\frac{1}{T_c(E)} - \frac{1}{T_c} = \frac{\chi_c}{b}\left(\frac{1}{\langle F^2\rangle/E^2 - 1}\right) \quad (4)$$

The critical temperature ($T_c(E)$) is raised for LCST solutions in the presence of electric field due to the negative value of b for LCST, but the degree of increase is too negligible to be considered. However, E has to be bigger than F in order to reduce $T_c(E)$ under the electric field. To arrive at this, F has to be decreased with increasing temperature as F depends on the temperature for a special blend system. Then, LCST depression is possible with increasing E from the temperature of $F < E$.

Since the PVDF/PBA blend is miscible in the entire blend composition ratio, one can consider it as a material having the volume of V, relative dielectric constant of ε, and no permanent dipole moment (P_0) under the pressure P. Assuming that the volume does not change when the electric field is applied to this material, the change in Gibbs free energy per unit volume ($\Delta G/V$) for this system can be expressed as shown in the following equation:[22,23]

$$\Delta G/V = -\frac{1}{2}\varepsilon_0\varepsilon E^2 \quad (5)$$

where ε_0 is the vacuum dielectric constant, E is the external electric field strength, and ε is the relative dielectric constant of the blend.

The free energy per segment in the absence of external electric field was expressed as sum of the segment−segment interaction energy H and the mixing entropy s. When the length and volume of segment for two polymers are different, the expression using the free energy of mixing for polymer−polymer blend per unit volume is more useful than that of free energy of mixing per unit segment. So the free energy of mixing for polymer (1)−polymer (2) blend per unit volume in the absence of electric field can be rewritten by the equation

$$\Delta G_m/V = RT\left(\frac{\phi_1}{V_1}\ln\phi_1 + \frac{\phi_2}{V_2}\ln\phi_2 + \chi\phi_1\phi_2\right) \quad (6)$$

where ϕ_1 and ϕ_2 are the volume fraction of polymer 1 and polymer 2, respectively, and V_1 and V_2 are the molar volume of polymer 1 and polymer 2, respectively, R is gas constant, and χ is the Flory−Huggins interaction parameter.

The free energy of mixing per unit volume ($\Delta G_m(E)/V$) under the electric field can be rewritten as eq 7, considering eq 5.

$$\Delta G_m(E)/V = RT\left(\frac{\phi_1}{V_1}\ln\phi_1 + \frac{\phi_2}{V_2}\ln\phi_2 + \chi\phi_1\phi_2\right) - \frac{1}{2}\varepsilon_0\varepsilon E^2 \quad (7)$$

Assuming that χ is independent of the concentration ϕ_2 and then differentiating eq 7 to the ϕ_2, the following equations are obtained.

$$\partial(\Delta G_m(E)/V)/\partial\phi_2 = RT[-1 + \ln(1-\phi_2)/V_1 + (1+\ln\phi_2)/V_2 + \chi(1-2\phi_2)] - \frac{1}{2}\varepsilon_0E^2(\partial\varepsilon/\partial\phi_2) \quad (8)$$

$$\partial^2(\Delta G_m(E)/V)/\partial\phi_2^2 = RT[1/(V_1(1-\phi_2)) + 1/(V_2\phi_2)] - 2\chi - \frac{1}{2}\varepsilon_0E^2(\partial^2\varepsilon/\partial\phi_2^2) \quad (9)$$

$$\partial^3(\Delta G_m(E)/V)/\partial\phi_2^3 = RT[1/(V_1(1-\phi_2)^2) - 1/(V_2\phi_2^2)] - \frac{1}{2}\varepsilon_0E^2(\partial^3\varepsilon/\partial\phi_2^3) \quad (10)$$

Assuming that $\varepsilon = n^2$ (n is the refractive index of blend) and $\partial n/\partial\phi_2 =$ a constant, the equations are given by

$$\partial\varepsilon/\partial\phi_2 = 2n(\partial n/\partial\phi_2) \quad (11)$$

$$\partial^2\varepsilon/\partial\phi_2^2 = 2(\partial n/\partial\phi_2)^2 \quad (12)$$

$$\partial^3\varepsilon/\partial\phi_2^3 = 0 \quad (13)$$

From the above equations, the critical composition ($\phi_{2,c}(E)$) and critical χ parameter ($\chi_c(E)$) are obtained in the conditions satisfying $\partial^2(\Delta G_m(E))/\partial\phi_2^2 = 0$ and $\partial^3(\Delta G_m(E))/\partial\phi_2^3 = 0$ simultaneously as follows:

$$\phi_{2,c}(E) = \frac{\sqrt{V_1}}{\sqrt{V_1}+\sqrt{V_2}} = \phi_{2,c}(0) \quad (14)$$

$$\chi_c(E) - \chi_c(0) \cong -\frac{\varepsilon_0E^2}{4RT_c(E)}\left(\frac{\partial^2\varepsilon}{\partial\phi_2^2}\right)_c \cong -\frac{\varepsilon_0E^2}{2RT_c(E)}\left(\frac{\partial n}{\partial\phi_2}\right)^2 < 0 \quad (15)$$

Knowing from eq 14, the critical composition ($\phi_{2,c}(E)$) under the electric field is equal to the critical composition ($\phi_{2,c}(0)$) in the absence of electric field, and the critical χ parameter ($\chi_c(E)$) is smaller than $\chi_c(0)$from eq 15.

On the other hand, $\chi(T)$ can be expressed as shown in eq 16.[1,11]

$$\chi(T) = a + \frac{b}{T} \quad (16)$$

For UCST (LCST), a is negative (positive) and b is positive (negative). Combining eq 16 with eq 15, eqs 17a and eq 17b are given by

$$1/T_c(E) - 1/T_c(0) \cong -\frac{\varepsilon_0 E^2}{2bRT_c(E)}\left(\frac{\partial n}{\partial \phi}\right)^2 \quad (17a)$$

$$\frac{T_c(E) - T_c(0)}{T_c(0)} \cong \frac{\varepsilon_0 E^2}{2bR}\left(\frac{\partial n}{\partial \phi}\right)^2 \quad (17b)$$

So the critical temperature ($T_c(E)$) is raised with electric field for UCST and the critical temperature ($T_c(E)$) decreases with electric field for LCST. From this, the explanation about descending LCST with increasing electric field becomes possible.

The binodal point becomes the point in which the two compositions have common tangential line in $\Delta G_m(E)/V$ vs ϕ_2 plot at the temperature, T, and one can get the binodal curve fitting to cloud point by using eq 8. So, to get the optimized fitting binodal curve, one has to obtain the values of a and b satisfying eq 16. However, one could not get the binodal and spinodal curves through curve fitting because one could not find the theoretical or experimental function expressed ε by ϕ_2.

The free energy of mixing per segment under the electric field obtained from Gurovich's theory (see eq 18a) is replaced by the free energy of mixing per unit volume as expressed in eq 18b.

$$\frac{\Delta G_m(\phi, E)}{kT} = \left[\frac{\phi}{x_1}\ln\phi + \frac{1-\phi}{x_2}\ln(1-\phi)\right] + \chi\left(1 - \frac{E^2}{\langle F^2\rangle}\right)\phi(1-\phi) \quad (18a)$$

$$\Delta G_m(E)/V = RT\left[\frac{\phi_1}{V_1}\ln\phi_1 + \frac{\phi_2}{V_2}\ln\phi_2 + \chi(1 - E^2/\langle F^2\rangle)\phi_1\phi_2\right] \quad (18b)$$

To get the binodal and spinodal curves using eq 18b, one should understand the theoretical/experimental equation about $\langle F^2\rangle$ as a function of temperature between two polymers. Only so, one could get the binodal and spinodal curves through fitting the cloud point. Thus, curve fitting to cloud point using this equation is not possible.

Assuming that the χ parameter depends on the temperature, blend composition, and electric field strength, $\chi(T,\phi_2,E)$ under the electric field can be expressed as eq 19

$$\chi(T, \phi_2, E) = a + b/T + c\phi_2/T \quad (19)$$

where a is the entropy coefficient depending on the electric field strength, b is the enthalpy coefficient depending on the electric field strength, and c is the enthalpy coefficient depending on the composition and electric field strength, the free energy of mixing per unit volume under the electric field can be rewritten as eq 20

$$\Delta G_m(E)/V = RT\left[\frac{\phi_1}{V_1}\ln\phi_1 + \frac{\phi_2}{V_2}\ln\phi_2 + \chi(T, \phi_2, E)\phi_1\phi_2\right] \quad (20)$$

In an earlier study on the temperature vs composition phase diagram of PVDF/PBA blends in the absence of electric field,[11] the calculated binodal line on the basis of Flory−Huggins theory was compared well with its experimental cloud point phase diagram. This also proved to be a useful aid in estimating the spinodal line to guide the experimental dynamics of phase separation in PVDF/PBA blends. In the present study, the fitted binodal and spinodal decomposition lines of PVDF/PBA blends calculated based on eq 20 were compared well with the experimental cloud point phase diagram for varying blend compositions under the electric field as shown in Figure 3. The critical temperature $T_c(E)$ is lowered with increasing electric field and $T_c(E)$ has the reducing tendency proportional to E^2 as confirmed further from Figure 4.

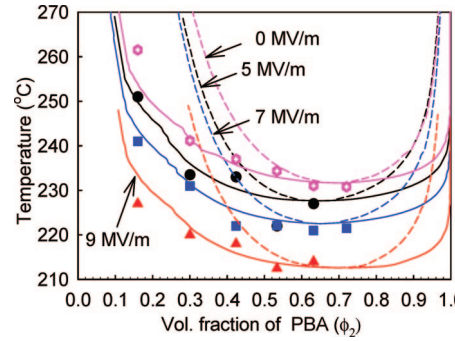

Figure 3. Fitted binodal and spinodal decomposition lines of PVDF/PBA blends calculated based on Flory−Huggins theory in comparison with the experimental cloud point phase diagram.

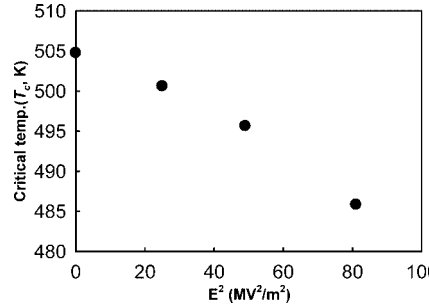

Figure 4. Critical temperature shift as a function of the square of the electric field strength for the PVDF/PBA blend.

Table 1. Thermodynamic Parameters Obtained from Curve Fitting

	0 MV/m	5 MV/m	7 MV/m	9 MV/m
a	7.50×10^{-4}	7.60×10^{-4}	7.657×10^{-4}	7.77×10^{-4}
b	−0.332	−0.331	−0.331	−0.331
c	−0.0118	−0.0150	−0.0140	−0.0130
T_c (°C)	231.76	227.61	222.65	212.84
$\phi_{2,c}$	0.692 01	0.640 83	0.653 99	0.664 56
χ_c	7.63×10^{-5}	7.983×10^{-5}	7.89×10^{-5}	7.813×10^{-5}

Table 1 depicts the thermodynamic parameters obtained from this curve fitting method. Entropy coefficient a and enthalpy coefficient c exhibit an increasing trend depending on the composition and electric field strength, whereas the enthalpy coefficient b shows almost similar values irrespective of increasing electric field. Since, with increasing electric field, the critical χ parameter is increased below 5 MV/m and is decreased above 5 MV/m, one cannot conclude that χ has a fixed correlation with an external electric field. Following eq 14, the critical composition $\phi_{2,c}(E)$ must be fixed regardless of electric field. However, $\phi_{2,c}(E)$ depends marginally on the electric field as observed experimentally. Nevertheless, one cannot surely determine a specific relationship between $\phi_{2,c}(E)$ and electric field strength. V_1 is the PVDF molecular weight × specific volume of PVDF, and V_2 is the PBA molecular weight × specific volume of PBA. So $\phi_{2,c}(0)$ calculated from eq 14 is 0.687 (from using $\sqrt{V_1}$ = 523 $(cm^3/mol)^{1/2}$ and $\sqrt{V_2}$ = 108 $(cm^3/mol)^{1/2}$). The calculated theoretical value is very much closer to the experimental results as shown in Table 1.

Electric-Induced Phase Separation and Electric Field Removal-Induced Phase Dissolution of PVDF/PBA Blends. As shown previously in Figure 2, the PVDF/PBA (9/1) blend without electric field at 246 °C (isothermal temperature) exists in the miscible region because this temperature is well below its cloud point (263 °C). Since the binodal point is lowered to

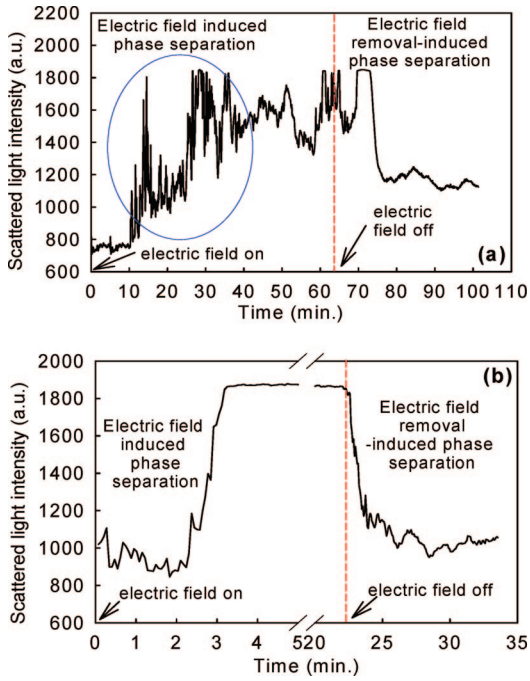

Figure 5. Changes in scattered light intensity as a function of time at isothermal temperature to find the electric field-induced phase separation and the electric field removal-induced phase dissolution of the PVDF/PBA blends. Electric field strength = 7 MV/m. (a) PVDF/PBA (9/1) at 246 °C and (b) PVDF/PBA (7/3) at 236 °C.

241 °C when applied with the electric field strength of 7 MV/m at 246 °C, it becomes immiscible due to phase separation at 246 °C. Figure 5a shows the electric field (7 MV/m)-induced phase separation behavior as observed from increasing scattered light intensity as a function of time (67 min) at 246 °C due to phase separation in PVDF/PBA (9/1) blend. When further increase in scattering intensity is not observed, the applied electric field is removed, thereby returning the binodal point to its original position. During this process, the scattering light intensity is decreased as a function of time due to the electric field removal-induced phase dissolution.

A closer look at the Figure 5a revealed the increasing scattered light intensity at around 10 min after applying electric field and reaching the saturated state after around 27 min. The resultant light scattering occurred due to the shifting of binodal curve to lower temperature (241 °C) under applied electric field (7 MV/m) and the resultant phase separation. This phenomenon is called the electric field-induced phase separation. After removing the electric field at around 67 min, the binodal curve is reversed to higher temperature with the unstable phase changing to a stable and single phase. Therefore, the scattered light intensity is also decreased as a function of time, and this phenomenon is called electric field removal-induced phase dissolution.

Figure 5b shows the changes in scattered light intensity as a function of time at 236 °C to study the electric field-induced phase separation and the electric field removal-induced phase dissolution of PVDF/PBA (7/3) blend using the same method as that applied for PVDF/PBA (9/1) blend. PVDF/PBA (7/3) blend exhibits a single phase at 236 °C (Figure 2). The scattered light intensity began to increase at around 2 min after applying electric field (7 MV/m) and reaches a saturated state after around 3 min. The scattered light intensity is reduced as the electric field is removed at around 22 min (Figure 5b). From this phenomenon, we can understand that the field-induced phase separation and the field removal-induced phase dissolution of PVDF/PBA (7/3) blend occur rather reversibly depending on the applied electric field.

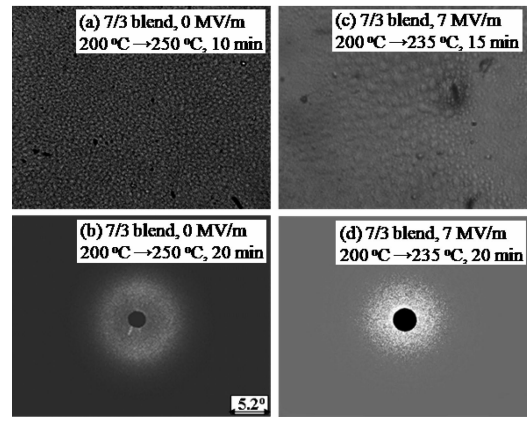

Figure 6. Optical micrographs and SALS patterns during spinodal decomposition following a *T*-jump experiment for the PVDF/PBA (7/3) blend with and without an electric field: (a) microscopic image revealing interconnected domains and (b) the corresponding scattering halo during spinodal decomposition following a *T*-jump from 200 to 250 °C without electric field; (c) microscopic image during spinodal decomposition following a *T*-jump from 200 to 235 °C with an electric field of 7 MV/m and (d) the corresponding scattering pattern.

Though the applied experimental temperature in PVDF/PBA (9/1) blend case is higher (246 °C) than the PVDF/PBA (7/3) blend case (236 °C), both the phase separation and phase dissolution rates for the former are slower than those of the latter, and the reason can be explained as follows: In the 9/1 blend case, the experimental temperature (246 °C) where the single phase is observed under the absence of electric field is only 5 °C higher than the binodal point of 241 °C observed under the electric field (7 MV/m). In the case of 7/3 blend, the experimental temperature (236 °C) where the single phase is observed under the absence of electric field is 14 °C higher than the binodal point of 222 °C observed under the electric field (7 MV/m). The electric field-induced phase separation and the electric field removal-induced phase dissolution occur faster in the 7/3 blend than in the 9/1 blend because the temperature gap from the binodal point observed under the electric field of 7 MV/m for the 7/3 blend is much larger than that for the 9/1 blend.

Morphology of PVDF/PBA Blends. Figure 6 shows the optical micrographs and SALS patterns during spinodal decomposition when temperature was jumped from a single phase to the two-phase state for the PVDF/PBA (7/3) blend with and without an electric field. Temperature-jump (*T*-jump) was carried out in the absence of electric field from 200 to 250 °C and under the applied electric field (7 MV/m) from 200 to 235 °C due to the shifting of binodal point to lower position. The optical microscopic image (Figure 6a) reveals interconnected domain of the two polymers, which is a typical spinodal phase separation result without electric field, and its 2-D SALS pattern (Figure 6b) also exhibits the traditional spinodal phase separation behavior by showing the traditional donutlike scattering pattern in the absence of electric field. But the optical image under the electric field (Figure 6c) shows a different type of phase separation image, and its 2-D SALS pattern (Figure 6d) does not show the donutlike scattering pattern, in contrast to that observed under the absence of electric field. One possible reason why the morphology developed through the phase separation under the electric field is quite different from that in the absence of the electric field can be explained as follows: The gyration of each component polymeric molecular chain in the melt state under the electric field does not form the round shape any longer. The polymeric molecular chain exhibits optical anisotropic property, since the gyration of polymer chain has an optical ellipsoidal indicatrix having a long axis parallel or vertical to

Table 2. Half-Crystallization Time ($t_{1/2}$) of the Isothermal Crystallization at 148 °C after Various Pretreatments of PVDF/PBA (7/3) Blend

sample no.	isothermal crystallization at 148 °C after various pretreatments of PVDF/PBA (7/3) blend	half-crystallization time ($t_{1/2}$, min)
1	210 °C (single phase)→ T_c (148 °C) (without an electric field)	13.1
2	210 °C (single phase) → T_c (148 °C) (with an electric field of 7 MV/m)	5.4
3	230 °C (single phase, soaking for 10 min without an electric field) → electric field-induced phase separation (soaking for 60 min with an electric field of 7 MV/m) → T_c (148 °C)	6.7
4	230 °C (single phase, soaking for 10 min without an electric field) → electric field-induced phase separation (soaking for 60 min with an electric field of 7 MV/m) → electric field removal-induced phase dissolution for 20 min → T_c (148 °C)	7.6
5	260 °C (two phase, soaking for 10 min) → T_c (148 °C) (without an electric field)	14.8

the electric field direction besides the phase separation based on thermodynamics.[20] Especially, the PVDF will show a more asymmetric optical indicatrix under the electric field than in the absence of it because the PVDF chain in the melt has more elongated or contracted gyration ellipsoid with increasing electric field. Another probable reason may be due to the inner part of the donut in Figure 6d partially hidden by the beam stop, resulting from quite coarser morphology than that observed in Figure 6b, but the exact reasons are not yet well understood.

Effect of Electric Field on the Crystallization Behavior after Spinodal Decomposition of PVDF/PBA Blends. For samples subjected to spinodal decomposition for enough time in a two-phase region of LCST for the amorphous/amorphous polymer blend, the desired morphology can be obtained by quenching below T_g at proper conditions. Interconnected void-like channel having uniform size can be formed by removing the other component using a solvent and membranes produced by this kind of technique are widely used to separate the molecules or particles of a certain size preferentially. The channel size depends on the degree of spinodal decomposition.[1] However, when the viscosity of the blend system is too low, the desired morphology obtained from adequate spinodal decomposition cannot be maintained at room temperature due to the phase dissolution during the quenching process. For samples quenched below the T_m from a two-phase region (above LCST and melting point) in the case of crystalline/amorphous blend system, it is not easy to maintain the morphology formed from spinodal decomposition because the crystallinity-induced phase separation also progresses along with the crystallization process. Moreover, for blend systems with very low viscosity, the prediction of final morphology is nearly impossible as phase dissolution and crystallization occur nearly at the same time, and the final morphology becomes much more complicated when the external electric field is additionally applied to this blend system.

From the previous section, the effect of electric field on the spinodal decomposition kinetics could not be investigated using the SALS technique because the typical scattering pattern corresponding to spinodal phase separation was not observed under the external electric field. Hence, this section focuses more on the effects of various pretreatment conditions (spinodal phase separation time, field-induced phase separation, field removal-induced phase dissolution, etc.) of the PVDF/PBA blend before isothermal crystallization on the crystallization kinetics. Based on the phase diagram of the PVDF/PBA (7/3) blend (Figures 2 and 3) under the electric field, the various pretreatments before isothermal crystallization at 148 °C were carried out as shown in Table 2. The reason to choose the crystallization temperature at 148 °C is that, since this temperature exists well below the binodal point of the 7/3 blend under the external electric field, the interesting phenomena caused by the simultaneous occurrence of phase dissolution and crystallization can be observed during cooling from a two-phase state to desired isothermal temperature. The degree of crystallinity with crystallization time was evaluated using the transmitted depolarized light intensity and the $t_{1/2}$ was also obtained to assess the relative crystallization rate.

After making a single molten phase state of PVDF/PBA (7/3) blend by heat treatment at 210 °C for 10 min, the sample was cooled to 148 °C (−20 °C/min) and crystallized isothermally at 148 °C. The crystallization occurs in a single phase since the crystallization temperature (148 °C) is below its binodal point, and the half-crystallization time ($t_{1/2}$) was 13.1 min in this case. On the contrary, PVDF-rich and PBA-rich phases are formed through spinodal decomposition by heat treatment at 260 °C for 20 min even though the two polymers are in liquid state, because the heat treatment temperature of 260 °C is above the spinodal point. This sample was crystallized isothermally at 148 °C after cooling from 260 °C, and for this case, the effect of phase dissolution occurring simultaneously should be considered. When the rate of crystallization is faster than that of phase dissolution or both phase dissolution and crystallization occurring simultaneously, the crystallization rate at the temperature of 148 °C (cooled from a two phase) should be faster than the crystallization at 148 °C (cooled from a single phase) because the crystallization takes place earlier in PVDF-rich phase.

On the contrary, when phase dissolution occurs earlier before crystallization process, the crystallization rate at 148 °C (cooled from a two phase) should be similar to that of crystallization rate at 148 °C for sample (cooled from a single phase). But the $t_{1/2}$ in case of crystallization at 148 °C after melting at 260 °C for 20 min is longer than that in case of crystallization at 148 °C after melting at 210 °C for 10 min. This may be due to the following reason: In the case of former, even tiny crystals are perfectly melted due to larger temperature range (85 °C) between 260 °C and T_m of PVDF and longer retention time (20 min), whereas, self-seeded crystals[24,25] may have existed due to the smaller temperature range (35 °C) between 210 °C and T_m of PVDF along with shorter retention time (10 min) resulting in shorter $t_{1/2}$ in the latter case.

For crystallization at 148 °C after melting at 210 °C for 10 min with an external electric field of 7 MV/m, $t_{1/2} = 5.4$ min is much shorter than that without an electric field. This result proves that electric field clearly affects the crystallization, and that the electric field assists the easier nucleation of PVDF. To study the effect of electric field on crystallization much more clearly, other crystallization experiments were conducted. After a single phase was obtained from heat treatment at 230 °C in the absence of an electric field, we carried out the field-induced phase separation by applying electric field of 7 MV/m for 60 min and then isothermal crystallization at 148 °C in the presence of the electric field ($t_{1/2} = 6.7$ min). In this case, the crystallization rate is slower when compared with sample crystallized at 148 °C after melting at 210 °C in the absence of an electric field. After the occurrence of field-induced phase separation in

the former case, the crystallization under an electric field occurs simultaneously with the phase dissolution. Usually, in cases where the phase dissolution occurs after the crystallization, the rate of crystallization from a two phase formed by field-induced phase separation can be predicted to be faster than the rate of crystallization from a single phase under the electric field due to the faster crystallization occurring in PVDF-rich phase. But, the experimental results from our studies are opposite to the prediction. On the contrary, in the cases where the phase dissolution starts earlier than the crystallization process, the rate of crystallization from a two phase should be similar to that of crystallization from a single phase under the electric field and our experimental results did not support this interpretation either. This may have resulted from the following reason: even tiny crystals would have perfectly melted due to longer retention time (70 min) and larger temperature range (55 °C) between 230 °C and T_m of PVDF, whereas traces of self-seeded crystals may have existed due to the smaller temperature difference (35 °C) between 210 °C and T_m along with shorter retention time (10 min) in a single phase under the electric field.

In another case, electric field-induced phase separation (7 MV/m, 60 min) was initially carried out in a single phase at 230 °C. Subsequent removal of the electric field for 20 min at the same temperature resulted in the electric field removal-induced phase dissolution which was followed by isothermal crystallization at 148 °C in the absence of electric field ($t_{1/2} = 7.6$ min). The $t_{1/2}$ is longer than in case of isothermal crystallization at 148 °C ($t_{1/2} = 6.7$ min) for the sample previously subjected to electric field-induced phase separation and considerably shorter when compared with isothermal crystallization at 148 °C ($t_{1/2} = 14.8$ min) for the phase-separated sample at 260 °C for 20 min. This indicates that the nucleation of PVDF occurs much faster due to remnant space charge in the blend system even though the electric field was removed after electric field-induced phase separation. Table 2 summarizes the $t_{1/2}$ obtained from various crystallization conditions.

IV. Conclusions

The effects of electric field on the phase separation behavior, crystallization morphology, and crystallization kinetics in PVDF/PBA blends have been studied. The phase diagram of PVDF/PBA blends showed the LCST and the miscibility of PVDF/PBA blends in the temperature range between the melting point of PVDF and the LCST. The binodal curve fitted with the cloud points obtained from light scattering measurement was shifted toward lower temperature in the presence of the electric field and confirmed with theoretical calculations. Compared to the PVDF/PBA (9/1) blend, the 7/3 blend exhibited lower miscible temperature and hence faster phase separation and dissolution rates, faster electric field-induced phase separation, and the electric field removal-induced phase dissolution rates due to the unstable thermodynamic condition caused by the shorter gap between its LCST and T_m of PVDF in PVDF/PBA blend. The effect of electric field on the spinodal decomposition kinetics could not be investigated using the SALS technique because the typical scattering pattern corresponding to spinodal phase separation was not observed under the external electric field. From the studies on crystallization kinetics, the isothermal crystallization rate of the PVDF/PBA (7/3) blend in the presence of an electric field was observed to be highly influenced by various pretreatment conditions like spinodal phase separation time, field-induced phase separation, and field removal-induced phase dissolution made before quenching to the isothermal temperature. Overall, the results obtained from this work were quite useful in understanding the effect of electrical field on the phase separation and crystallization behavior of PVDF/PBA blends, and the experimental observations were in fairly good agreement with the trends predicted from our theoretical calculations.

Acknowledgment. This study was supported by the Korea Science and Engineering Foundation (KOSEF Grant No. R01-2000-00339), "The National Research Program for the 0.1 Terabit Nonvolatile Memory Development sponsored by Korea Ministry of Commerce, Industry and Energy", and Korea Science and Engineering Foundation (KOSEF) through the SRC/ERC Program of MOST/KOSEF (R11-2005-065).

References and Notes

(1) Olabisi, O.; Robeson, L. M.; Shaw, M. T. *Polymer-Polymer Miscibility*; Academic Press: New York, 1979.
(2) Coleman, M. M.; Painter, P. C.; Graf, J. F. *Specific Interactions and the Miscibility of Polymer Blends*; Technomic: Lancaster, PA, 1991.
(3) Reich, S.; Gordon, J. M. *J. Polym. Sci., Polym. Phys. Ed.* **1979**, *17*, 371–378.
(4) Kumaki, J.; Hashimoto, T. *Macromolecules* **1986**, *19*, 763–768.
(5) Kyu, T.; Saldanha, J. M. *Macromolecules* **1988**, *21*, 1021–1026, and references therein.
(6) Kyu, T.; Lim, D. S. *Macromolecules* **1991**, *24*, 3645–3650.
(7) Nishi, T.; Wang, T. T. *Macromolecules* **1975**, *8*, 909–915.
(8) Tomura, H.; Saito, H.; Inoue, T. *Macromolecules* **1992**, *25*, 1611–1614.
(9) Walker, T. A.; Melnichenko, Y. B.; Wignall, G. D.; Spontak, R. J. *Macromolecules* **2003**, *36*, 4245–4249.
(10) Penning, J. P.; Manley, R. S. J. *Macromolecules* **1996**, *29*, 77–83.
(11) Fujita, K.; Kyu, T.; Manley, R. S. J. *Macromolecules* **1996**, *29*, 91–96.
(12) Okabe, Y.; Kyu, T.; Saito, H.; Inoue, T. *Macromolecules* **1998**, *31*, 5823–5829.
(13) Isayeva, I.; Kyu, T.; Manley, R. S. J. *Polymer* **1998**, *39*, 4599–4608.
(14) Kim, K. J.; Kyu, T. *Polymer* **1999**, *40*, 6125–6134.
(15) Liu, J.; Jungnickel, B. J. *J. Polym. Sci., Polym. Phys.* **2007**, *45*, 1917–1931, and references therein.
(16) Wirtz, D.; Berend, K.; Fuller, G. G. *Macromolecules* **1992**, *25*, 7234–7246.
(17) Wirtz, D.; Fuller, G. G. *Phys. Rev. Lett.* **1993**, *71*, 2236–2239.
(18) Gurovich, E. *Macromolecules* **1994**, *27*, 7063–7066.
(19) Gurovich, E. *Macromolecules* **1994**, *27*, 7339–7362.
(20) Gurovich, E. *Macromolecules* **1995**, *28*, 6078–6083.
(21) Paul, D. R.; Barlow, J. W.; Bernstein, R. E.; Wahrmund, D. C. *Polym. Eng. Sci.* **1978**, *18*, 1225–1234.
(22) Guggenheim, E. A. *Thermodynamics*, 5th ed.; North-Holland: Amsterdam, 1967.
(23) Marand, H. L.; Stein, R. S.; Stack, G. M. *J. Polym. Sci., Polym. Phys. Ed.* **1988**, *26*, 1361–1383.
(24) Li, Y.; Kaito, A. *Macromol. Rapid Commun.* **2003**, *24*, 603–608.
(25) Toda, A.; Kojima, I.; Hikosaka, M. *Macromolecules* **2008**, *41*, 120–127.

MA702655N